ORIGINAL PAPER

Multiscenario flood hazard assessment using probabilistic runoff hydrograph estimation and 2D hydrodynamic modelling

Rita Tufano[1] · Luigi Guerriero[1] · Mariagiulia Annibali Corona[1] ·
Giuseppe Cianflone[2] · Diego Di Martire[1] · Fabio Ietto[2] · Alessandro Novellino[3] ·
Concetta Rispoli[1] · Claudia Zito[1] · Domenico Calcaterra[1]

Abstract

In this paper, we aim to define a procedure of flood hazard assessment applicable to large river basins in which flood events can be induced/sustained by the full basin area or by fractions of the total area as functions of the extent of the triggering precipitation event. The proposed procedure is based on a combined approach accounting for (1) the reconstruction of intensity–duration–frequency curves expressing the magnitude in terms of intensity for multiple return periods; (2) the application of the soil conservation service method for runoff estimation from a selected rainfall scenario considering some characteristics of the basin (i.e. soil type, land use/treatment, surface condition, and antecedent moisture conditions); (3) 2D hydrodynamic modelling conducted by the HEC-RAS model using runoff hydrographs as hydrological input data; (4) the reconstruction of flood hazard maps by overlaying multiple inundation maps depicting flood extent for different return periods. To account for the variability in the extent of the triggering precipitation event and the resulting input hydrograph, multiple contributing areas are considered. The procedure is tested at the archaeological site of Sybaris in southern Italy, which is periodically involved in flood events of variable magnitude. The obtained results highlight that the variable extent of the floodable area is strongly conditioned by the extent of the contributing area and return period, as expected. The archaeological site is always involved in the simulated flooding process, except for the smallest contributing area for which only a 300-year event involves this part of the site. Our findings may be useful for developing and supporting flood risk management plans in the area. The developed procedure might be easily exported and tested in other fluvial contexts in which evaluations of multiple flood hazard scenarios, due to the basin geometry and extent, are needed.

Keywords Flood hazard map · SCS-CN method · Hydrodynamic model · Hazard scenario · Cultural heritage · Sybaris · Archaeological site

✉ Luigi Guerriero
   luigi.guerriero2@unina.it

Extended author information available on the last page of the article

1 Introduction

Flooding is considered one of the most disastrous phenomena that affect many parts of the world, causing losses of human lives and infrastructure and property damage (Teng et al. 2017; Mokhtar et al. 2018). Flood events can be induced by both short-duration and high-intensity or prolonged and low-intensity rainfall events. Due to climate change, local intense rainfall is becoming increasingly frequent, resulting in a rapid increase in river levels that contribute to fluvial/riverine floods. In urban environments, such events induce pluvial floods in the case of excessive runoff caused by exceeding the capacities of drainage systems (Lin et al. 2019). To define flood hazard (FH) and related zones, inundation maps depicting water depths related to the characteristic return periods of triggering events (i.e. rainfall) are usually considered. The boundary condition for this evaluation is a reference scenario generally corresponding to an extreme flood event (Woo and Waylen 1986). This reference extreme flood scenario is commonly identified based on hydrological historical data (i.e. rainfall or discharge data, e.g. Sutcliffe 1987), or, in their absence, on geomorphological field observations (e.g. Furdada et al. 2008; Magliulo and Cusano 2016; Montané et al. 2017). Comprehensive analyses of hazards that provide information on the magnitude and frequency levels of events allow for evaluating the risks and quantitatively estimating the expected annual damage induced by a specific event. For this purpose, in recent years, many countries have produced flood risk maps for their territories considering a specific return period range. In Italy, following the European Flood Risk Directive 2007/60/EC of 2007, the Ministry of Environment and Land Protection (now the Ministry of the Ecological Transition) has provided guidelines for implementing FH and risk maps at the hydrographic basin scale.

Recently, many methodologies have been developed for FH assessment to improve predictions of the spatial extent, depth of water level, and flood frequency (e.g. Cook and Merwade 2009; Ongdas et al. 2020; Kim et al. 2021). Empirical models are often based on various statistical and data-driven approaches; they can be categorized into several methods, such as multicriteria analysis (e.g. Chen et al. 2014), which is developed using multiple indicators based on statistical laws and expert knowledge; statistical methods (e.g. Nuswantoro et al. 2016; Guerriero et al. 2020a, b), which include bivariate (e.g. Youssef et al. 2015; Costache 2019; El-Magd 2019) and multivariate (e.g. Shafizadeh-Moghadam et al. 2018; Tien Bui et al. 2019) models; and machine learning methods (e.g. Wang et al. 2015; Al-Abadi 2018; Janizadeh et al. 2019; Costache 2019; Rahman et al. 2019). In general, the empirical approach may be associated with significant uncertainty due to the unavailability of sufficient historical data and high-quality field records (Lin et al. 2019; Tufano et al. 2019). Numerical hydrologic and hydrodynamic models (e.g. Liang et al. 2016; Wang and Yang 2020) simulate physical hydrological processes leading to flooding events through scenario simulation analyses (Bates and De Roo 2000; Di Baldassarre et al. 2010; De Risi et al. 2015; Gonçalves et al. 2015; Toda et al. 2017). Although numerical models require a significant amount of input data (Tufano et al. 2016, 2021) and are usually applied to small areas to replicate the physical processes behind water flow (Ji et al. 2012; Chen et al. 2016; Carmo 2020), they provide effective results that allow us to better understand the hydrological processes associated with flooding generated by rainfall (Rashid et al. 2016). In this context, hydrological input data are generally represented by runoff hydrographs. Hydrographs are often not directly available due to a lack of gauging stations, but multiple techniques have been developed to estimate synthetic unit

hydrographs representative of river dynamics (Salami et al. 2017). One of the most common event-based rainfall–runoff methods is the soil conservation service curve number (SCS-CN) method (SCS 1956, 1964, 1972, 1993), for which the peak discharge of stream flow is obtained from a synthetic unit hydrograph for a given rainfall event through convolution. Due to the spatiotemporal variability of rainfall, the quality of measured rainfall data, and the variability of watershed characteristics (i.e. soil type, land use, surface condition, and antecedent soil moisture), the SCS-CN method can exhibit variability in runoff computations (Ponce and Hawkins 1996).

In large river basins, flood events induced by rainfall can be sustained by contributing areas of variable extent as functions of the spatial concentrations of the triggering meteorological events. Flood hazard assessment at the basin scale often considers flood events generated by the overall basin extent; therefore, the potential for events sustained by a fraction of the basin surface is not considered. This consequence might represent a limitation in the evaluation since, in such systems, the magnitude of a flood is related to both the return period and spatial extent of the triggering rainfall event. Deriving multiple flood hazard scenarios might be significant, especially when associated with a statistic of flood-contributing areas for the selected basin. On this basis, in this paper, a multiscenario flood hazard estimation procedure accounting for the potential variability levels of contributing areas in rainfall-induced flood development is presented and tested. The procedure is based on a probabilistic analysis of a long-term rainfall series of annual maxima for intensity–duration–frequency (IDF) curve generation, followed by surface runoff estimation by the SCS-CN rainfall–runoff method considering extents and characteristics of multiple contributing areas, hydrodynamic modelling through the hydrologic engineering centre river analysis system (HEC-RAS) model, and finally, flood hazard map production by inundation scenario overlay.

To test its potential, this procedure is applied to the archaeological site of Sybaris (southern Italy), which represents the most important Archaic Greek settlement of Magna Graecia in southern Italy and is in a floodplain susceptible to floods (Petrucci and Polemio 2007). This site has been involved in several destructive riverine flood events, such as those that occurred in 2013 and 2018. The choice of this site is based on the growing attention to the protection of cultural heritage sites from geological phenomena and the ongoing need for specific methodologies supporting risk evaluation and mitigation measurement planning for these cultural assets (Iriarte et al. 2010; Jigyasu et al. 2014; Rispoli et al. 2020; Valagussa et al. 2020). Especially in Italy, out of a total of 205,670 cultural heritage sites, approximately 16,000 sites (~8% of the total) are exposed to high flood hazards. Of these, 804 sites are in the Calabria region of southern Italy (Trigila et al. 2021). The results from procedure application indicate (1) its potential in supporting the understanding of the hydrological processes behind flood initiation, (2) the reliability of predictions of the rainfall–runoff processes, and (3) the significance of simulating the dynamics of overland flows in flood hazard estimation.

The paper is structured as follows: Sect. 2 provides an overview of the test site. The methods section describes the probabilistic rainfall and discharge analyses (which are used to derive different scenarios of the event), the SCS-CN method for runoff hydrographs estimation, the hydrodynamic model HEC-RAS, and the application of the approach to the study area. In Sect. 4, the obtained results are described and discussed. In Sect. 5, the obtained results are validated, and Sect. 6 provides concluding remarks.

2 Study site

The test site selected for the application of the developed procedure is the Sybaris archaeological site located approximately three kilometres from the Crati River mouth in the alluvial plain of Sibari, in southern Italy (Fig. 1a). From a geological point of view, the plain is between the Calabrian Arc and Southern Apennines within a complex geologic context characterized by the overlapping of thin Calabrian Arc units on the Apennine units. Calabrian Arc units, which are outcropped along the southern margin, consist of various igneous and metamorphic rocks (Liberi and Piluso 2009), while Apennine units are composed of a Mesozoic-Tertiary carbonate succession and flysch deposits overlapped by a Plio-Pleistocene siliciclastic succession (Selli 1962; Caruso et al. 2013). The Sibari Plain originated from tectonic activity (Pliocene–lower Pleistocene; Ambrosetti et al. 1987) and was subsequently filled by fan deltas and marine terrigenous sediments. In particular, the upper part is occupied by Holocene alluvial deposits, mostly originating from rivers that cross the plain (e.g. Crati River), with a maximum thickness estimated up to ~ 100 m (Cianflone et al. 2018). The consolidation process is responsible for the strong subsidence (~ 3 mm/year) that affects the plain, both in historical and present times (Ferranti et al. 2011; Cianflone et al. 2015). In the past, the plain was characterized by very active fluvial dynamics, including different stream captures and drainage diversions, as testified by the numerous paleoriverbeds in the area (Cianflone et al. 2018).

The main river that crosses the plain is the Crati. Its basin is 2460 km^2 wide, with a mean discharge at the mouth of ~ 36 m^3/s and a torrential regime with alternating abrupt, high-discharge flood periods and dry periods in the summer season. The Crati is affected by the presence of some artificial lakes along its course (i.e. Tarsia and Esaro dams), while artificial embankments along its lower course limit flood potential. Due to the wide extension of the Crati Basin, it contains many tributaries, the most important of which are the Coscile and Esaro Rivers, with mean discharge levels of ~ 14 m^3/s and 8.9 m^3/s, respectively.
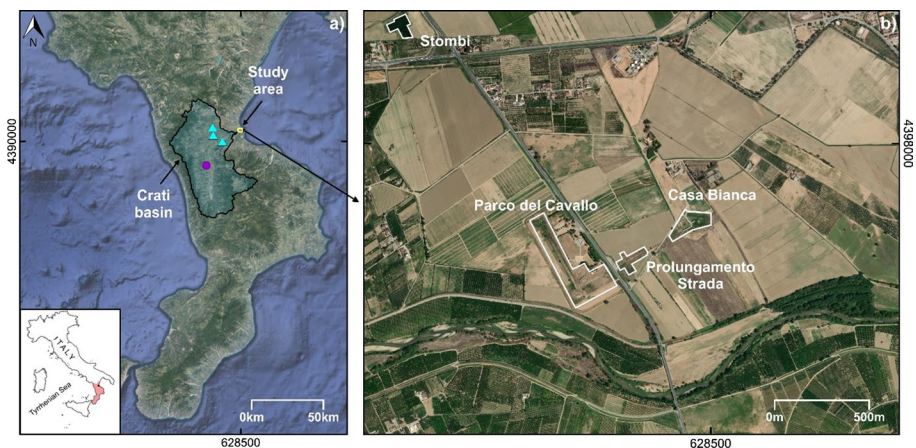

Fig. 1 **a** General framework of the study area with the indication of the Crati Basin (purple circle indicates the Torano Scalo rain gauge; cyan triangles indicate the Crati, Coscile, and Esaro hydrometric stations). **b** Position and structures of the Sybaris archaeological site.

The Sybaris archaeological site is in the ancient Greek town of Sybaris, founded in 720 B.C. Sybaris is considered among the most important archaeological finds of the Archaic and Classical ages in the Mediterranean area. After the decline of Sybaris in approximately 500 B.C., the Hellenist town of Thurii (approximately 440 B.C.) and the Roman town of Copia (approximately 190 B.C.) were successively developed, overlapping the remnants of the older towns (Greco et al. 1999). The most recent of the three is better represented within the archaeological site due to its position near the ground surface. Historic outcropped settlements are diffused over the four major sectors of the site: the Parco del Cavallo, the Prolungamento Strada, the Casa Bianca, and the Stombi (Fig. 1b).

Moreover, due to its low topographic position (between 2 and 6 m below the ground surface), the ongoing subsidence (Cafaro et al. 2013; Bianchini and Moretti 2015; Cianflone et al. 2015), and the proximity to the coastline, the site is susceptible to groundwater flooding events, which are prevented by a set of well points that continuously work to maintain the water table below the level of the archaeological site.

3 Materials and methods

As reported in Fig. 2, the proposed procedure of multiscenario flood hazard assessment is based first on the probabilistic analysis of rainfall time series to reconstruct IDF curves. Second, this assessment is based on the curve number (CN) estimated on the basis of land use, hydrologic soil group (HSG), and antecedent moisture conditions (AMC) of soils. Considering multiple contributing areas, the procedure consists of runoff hydrographs calculation by the SCS-CN method and the hydrodynamic modelling by the HEC-RAS model, providing maps of depth and extension of flow. Finally, the approach is based on FH maps assembled by overlaying the flood inundation maps.
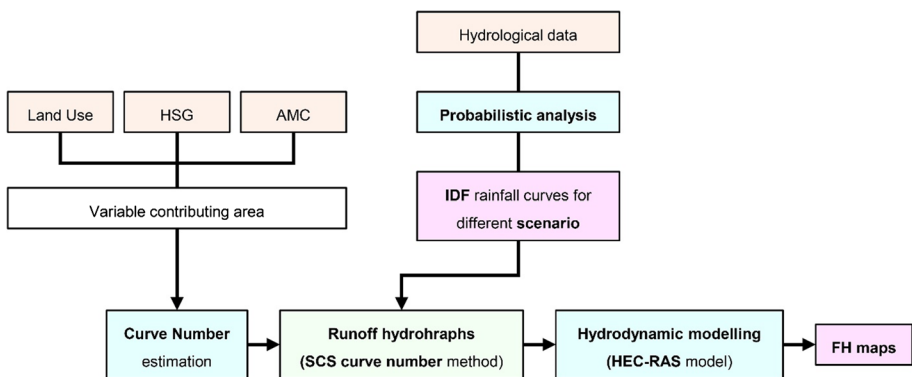

Fig. 2 Flowchart of methodologies applied for FH mapping

4 FH estimation

4.1 Probability analysis of hydrological data

As a first step for FH estimation, the annual maximum rainfall data were fit by the type I generalized extreme value (GEV) distribution (Gumbel; e.g. Jenkinson 1955) for a specific return period. The probability function F(h) was expressed as follows:

$$F(h) = \exp\{- \exp[-(\alpha(h - u))]\} \tag{1}$$

where h is the maximum rainfall height and the parameters α and u are estimated considering the mean value of the series (μ) and its standard deviation (σ), respectively. They were calculated through the following equations:

$$\alpha = \frac{1.283}{\sigma} \tag{2}$$

$$u = \mu - 0.45\sigma. \tag{3}$$

F (h) represents the probability of not exceeding the value of the rainfall height h by a random variable. Fixed a return period $T > 1$, the inverse of the cumulative distribution function (CDF; i.e. a survivor distribution function) provides the values of h on the basis of the return period T and duration d:

$$h(d) = u(d) - \frac{1}{\alpha(d)} \ln\left(-\ln\left(1 - \frac{1}{T}\right)\right). \tag{4}$$

Equation (4) allows us to define the height–duration–frequency (HDF) curves of rainfall, generally described as follows:

$$h(d, T) = a(T)d^n \tag{5}$$

where a and n are parameters estimated through a graphical and probabilistic approach, respectively.

IDF curves were derived directly by HDF curves for the selected return periods of (1) 10 years, (2) 50 years, (3) 100 years, and (4) 300 years.

Conversely, the annual discharge data were fit by a gamma distribution function (e.g. Yue 2001; Guerriero et al. 2018) to estimate the probability of exceedance (p) and the related return period (T). The related return period had the following form:

$$F(x) = \frac{\beta^\alpha x^{\alpha-1} e^{-\beta x}}{\Gamma(\alpha)} \tag{6}$$

where x is the maximum discharge, α is the shape, β is the scale parameter of distribution, and $\Gamma(\alpha)$ is the gamma function, which was calculated as follows:

$$\Gamma(\alpha) = \int_0^x x^{\alpha-1} e^{-x} dx \tag{7}$$

As indicated by Guerriero et al. (2020b), the generalized extreme value distribution function was suitable for describing the statistical behaviours of annual maxima; however, it had

the disadvantage of underestimating the intensities of very high-return period events. For this reason, the gamma function could be useful to overcome this drawback, especially for time series presenting problems with continuity and length.

4.1.1 Rainfall–runoff model description for hydrograph estimation

The SCS-CN method (SCS 1956, 1964, 1972, 1993) is adopted for constructing synthetic unit hydrographs based on a dimensionless hydrograph, which relates ratios of time to ratios of flow (for more details, see Ramírez 2000). The method is based on the following equation:

$$\frac{P - I_a - Q}{S} = \frac{Q}{P - I_a} \tag{8}$$

where P is the cumulative rainfall (mm), I_a is the initial abstraction (mm), Q is the runoff and S is the potential maximum soil moisture retention after runoff initiation (mm). With respect to runoff, Eq. (8) takes the following form:

$$Q = \frac{\left(P - I_a\right)^2}{\left(P - I_a\right) + S} \tag{9}$$

Further simplifications of the SCS-CN method are represented by the average value for I_a, which is selected as 0.2S, and by the introduction of a parameter called curve number (CN):

$$S = \left(\frac{1000}{CN} - 10\right). \tag{10}$$

CN varies between 30 for low runoff potential (and high infiltration) and 100 for high runoff potential, depending on land use, HSG, and AMC. Four HSGs to account for the infiltration abilities of different soils are considered: Group A (low runoff potential); Group B (moderate infiltration rates); Group C (slow infiltration rates); and Group D (high runoff potential). Once the group is defined, CN is evaluated based on land use. Moreover, due to the variability in the antecedent rainfall conditions and the associated soil moisture amount, the CN value exhibits variability in the recognition of the AMC. Specifically, three levels of AMC could be considered: AMC I (dry), AMC II (normal), and AMC III (wet). From a statistical point of view, AMC I, AMC II, and AMC III correspond to 90, 50, and 10% cumulative probability of exceedance of runoff depth for a given rainfall, respectively (Hjemfelt et al. 1982).

The synthetic unit hydrograph is expressed as the ratio of runoff Q and peak of discharge Q_p, and the ratio of time t (duration of rainfall) and time to peak t_p (Ramírez 2000). The ratio of Q to Q_p increases over time and reaches a maximum value (equal to 1) when Q equals Q_p; then, it decreases until it reaches a value near zero. The time required to reach the peak and return to zero defines the duration of the hydrograph.

The peak discharge, modulated by the basin area (a) and runoff (Q), is obtained through the equation:

$$Q_p = \frac{0.208 \times a \times Q}{t_p}. \tag{11}$$

The time to peak t_p is calculated as follows:

$$t_p = \frac{t_c + 0.133t_c}{1.7} \qquad (12)$$

where t_c is the time of concentration (min).

In the technical literature, there are several empirical equations for estimating the time of concentration with good applicability levels because of the limited information they require.

The values of both the peak discharge and time to peak are applied to the dimensionless hydrograph ratios by the SCS-CN method, allowing us to obtain a unit hydrograph (e.g. Raghunath 2006). Subsequently, the established unit hydrograph is used to develop run-off hydrographs considering cumulative rainfall derived by IDF curves for selected return periods.

Moreover, due to the uncertainty linked to the spatial concentrations of the triggering meteorological events, three variable contributing areas are considered. For this purpose, a topographic analysis is conducted in a GIS environment to delineate a defined watershed area. The algorithm used is an eight-direction pour point algorithm that starts from the digital elevation model (DEM) of the area and the drainage network.

4.1.2 2D hydrodynamic modelling

Runoff hydrographs developed considering IDF curves and contributing area features are used for multiscenario hydrodynamic simulations conducted through the HEC-RAS model (Brunner 2021). The software simulates the movement of water over a topographic surface by solving the Saint–Venant equations:

$$\frac{\delta A}{\delta t} + \frac{\delta Q}{\delta x} = q_l \qquad (13)$$

$$\frac{\delta Q}{\delta t} + \frac{\delta \left(\frac{Q^2}{A} \right)}{\delta x} + gA\frac{\delta H}{\delta x} + gA\left(S_0 - S_f \right) = 0 \qquad (14)$$

where A is the cross-sectional area normal to the flow, Q is the discharge, g is the acceleration due to gravity, H is the water surface elevation, t is the temporal coordinate, x is the longitudinal coordinate, q_l is lateral inflow from tributaries (in our case equals 0), S_0 is the channel bottom slope, and S_f is the friction slope. Equations (13) and (14) are solved using the four-point implicit box finite difference scheme.

4.2 Application of the proposed procedure to the Sybaris archaeological site

The proposed procedure of FH analysis was tested through an application at the archaeological site of Sybaris. To this end, the data collected for the study area consisted of: long rainfall time series, three discharge time series, a 5×5 m DEM, the Crati Basin drainage network, and a land use map.

Rainfall data (Fig. 3a), in the form of annual maxima for specific durations (1, 3, 6, 12, and 24 h), were derived by the Torano Scalo rain gauge (see Fig. 1a for position) measurements, recorded between 1934 and 2012 (https://www.cfd.calabria.it/). There were 60 units of data, and discontinuities were present; therefore, only the data between 1962 and 2012 (41 units) were considered. Discharge data (Fig. 3b–d) in the form of annual maxima
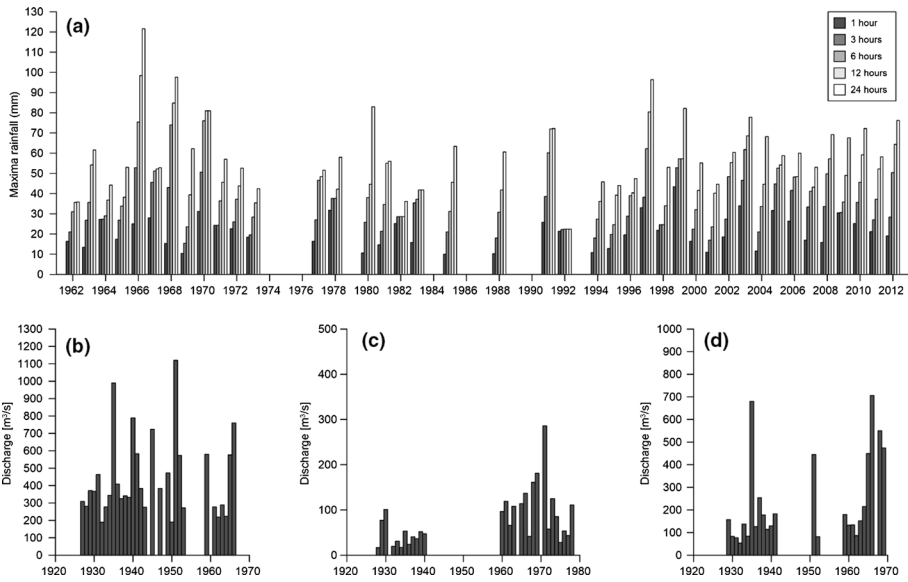
Fig. 3 Annual maximum rainfall for given durations of 1 h, 3 h, 6 h, 8 h, 12 h and 24 h starting from 1962 to 2012, derived by the Torano Scalo rain gauge (**a**); discharge time series recorded by the hydrometric stations at the Crati River from 1927 to 1966 (**b**), Coscile River from 1928 to 1978 (**c**), and Esaro River from 1929 to 1969 (**d**)

were derived by the Crati, Coscile, and Esaro stations (see Fig. 1a for position), recorded between 1927 and 1966 (31 units) for the Crati station, 1928 and 1978 (29 units) for the Coscile station, and 1929 and 1969 (25 units) for the Esaro station. The 5×5 m DEM was provided by the Centro Cartografico Regione Calabria and the drainage network by the Agenzia Regionale per la Protezione dell'Ambiente (ARPACAL) website (https://www.cfd.calabria.it/); the land use map was derived by Corine Land Cover-2018 (EEA 2020).

Probabilistic analyses were conducted on the annual maxima of rainfall time series by using the inverse Gumbel distribution function, with the aim of estimating the IDF curves, while the peak discharge values for specific return periods were estimated by conducting probabilistic analyses of the annual maxima of discharge time series by using the gamma distribution function. With the first analysis, the runoff–rainfall model considered (SCS-CN method) was able to generate runoff hydrographs on the basis of the parameters estimated by Eqs. 8–12: the runoff Q; the peak of discharge Q_p; the time t intended as the duration of rainfall and derived by IDF curves; and the time to peak t_p. To estimate the latter, it was necessary to calculate the concentration time t_c, which, due to the large size of the analysed basin, required the application of multiple equations to derive a mean value. The relationships used were SCS-CN (SCS 1956), Ventura (1905), Giandotti (1934), Pezzoli (Indelicato 1988), Puglisi (Puglisi and Zanframundo 1978), and Tournon (Merlo 1973).

The contributing areas considered were obtained on the basis of specific thresholds of the drainage areas. We considered three contributing areas corresponding to (A) the entire extension of the Crati Basin; (B) an estimated contributing area of 1016 km^2 based on a threshold of the drainage area of 1000 km^2; and (C) an estimated contributing area of 286 km^2 based on a threshold of the drainage area of 100 km^2. The geomorphological parameters (i.e. extent, average slope, maximum, average and minimum elevation, length, and average slope) of the contributing area selected are reported in Table 1. Table 2 reports the

Table 1 Contributing area characteristics

Features of the basin	A	B	C
Area (km^2)	2447.7	1016.0	286.0
Average slope (%)	24.97	27.70	27.60
Maximum elevation (m a.s.l.)	2240.0	2240.0	1080.0
Average elevation (m a.s.l.)	595.8	492.1	285.6
Minimum elevation (m a.s.l.)	0.0	16.0	16.0
Main stream length (km)	89.9	54.5	35.4
Main stream slope (–)	0.50	0.19	0.07

Table 2 Concentration time t_c in hours for the contributing areas A, B, and C estimated by using different empirical equations

Equation	Concentration time (h)		
	Area A	Area B	Area C
SCS curve number	12.3	7.8	5.5
Ventura	8.9	9.3	8.1
Giandotti	17.0	11.8	8.9
Pezzolli	7.0	6.9	7.3
Puglisi	5.1	3.6	3.5
Tournon	5.2	3.8	2.1
Average value	9.3	7.2	5.9

The average value is shown

values of t_c estimated by different relationships for each contributing area. The calculated mean value was finally used to calculate the t_p.

Regarding the estimation of CN, considering different extensions of the contributing areas, a unique value was derived for each of these areas on the basis of the land use map (Fig. 4). For each of them, the HSG was the B group, and AMC was assumed to be class II due to the lack of information for the study site. Table 3 shows the CN values attributed to different land use areas in the Crati River Basin. The weighted average value of CN used for the analysis was estimated to be ~73 for all three contributing areas.

Finally, for modelling purposes, the 2D hydrodynamic simulations were set in the HEC-RAS model taking into account a computational cell size of 20×20 m considering the computational power required for the modelling. The boundary conditions were defined considering one inflow cell located within the Crati River on the upper boundary of the computational area and outflow cells located along the coastline and the upper and lower boundary of the computational area (Fig. 5).

The channel's Manning's roughness coefficient n was set at 0.03 m$^{-1/3}$×s according to the type of channel simulated (natural channel; Chow 1959). The hydrodynamic simulation was run considering the developed 47-h (area A)-, 40-h (area B)-, and 30-h (area C)-long hydrographs over a total simulation time of 120 h. The outputs generated inundation maps in terms of the flow depth and extent for each return period considered. FH maps were obtained by combining the inundation maps for the poorest inundation condition of each contributing area, from the lowest layer corresponding to a 300-year event to the
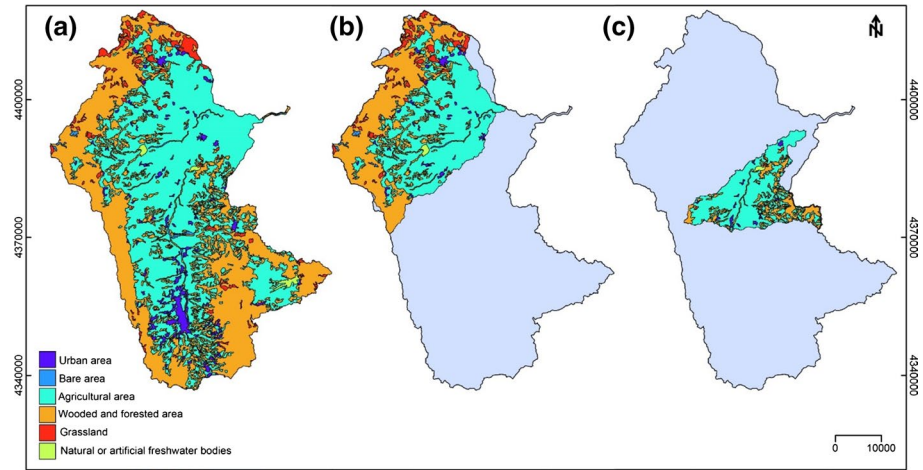
Fig. 4 Land use maps for the contributing areas: **a** A, **b** B and **c** C

Table 3 CN values of contributing areas A, B and C

Description	CN (–)
Wooded and forested area	73
Grassland	69
Agricultural area	74
Urban area	88
Bare area	88
Freshwater bodies	–

highest layer corresponding to a 10-year event. Since the analysis was completed through a reduced complexity approach, the flow velocity was not considered in the FH estimation.

5 Results and discussion

Figure 6 shows IDF curves obtained for the selected return periods, indicating the maxima intensities of 59.3 mm/h, 52 mm/h, 47.4 mm/h, and 36.4 mm/h for return periods of 300 years, 100 years, 50 years, and 10 years, respectively, with a critical duration of 1 h. Conversely, the minimum values, which were identified for a critical duration of 24 h, were 6.9 mm/h, 6.1 mm/h, 5.6 mm/h, and 4.3 mm/h for return periods of 300 years, 100 years, 50 years, and 10 years, respectively.

Considering the estimated runoff, rainfall implemented in the SCS-CN method was identified as the amount corresponding to critical duration, which in this case was equal to the time of concentration t_c for each contributing area. For the mean t_c estimated at 9.3 h, 7.2 h, and 5.9 h for contributing areas A, B, and C, respectively (Table 2), Table 4 provides the amount of rainfall calculated on the basis of these critical durations (i.e. the t_c). This amount represented the term P in the Eqs. 8 and 9.
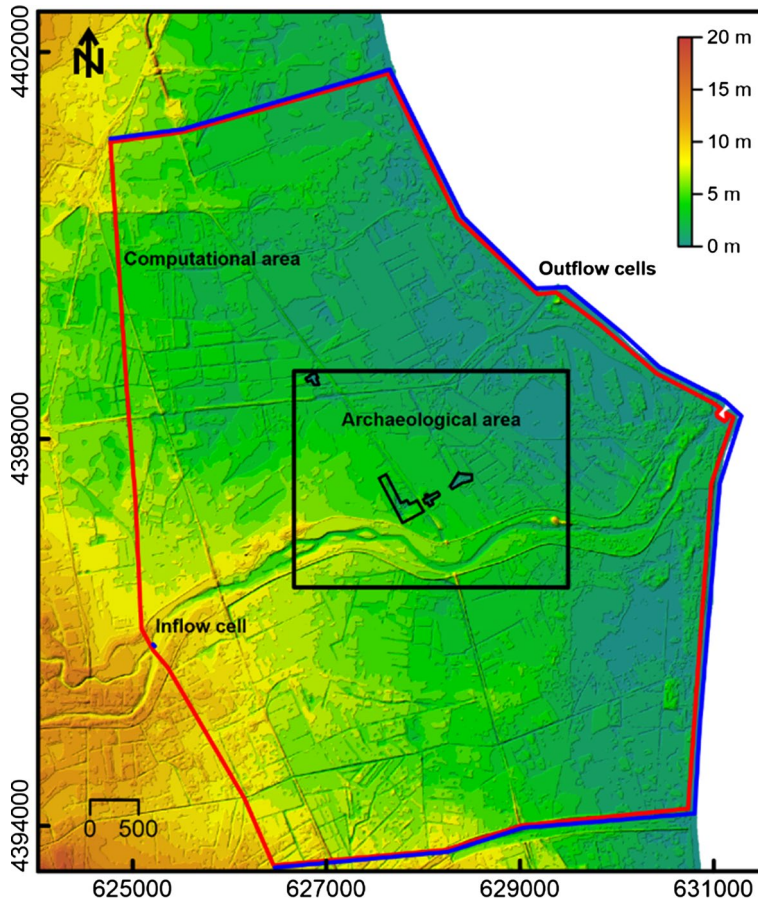
Fig. 5 Computational scheme of the hydrodynamic modelling. The figure shows the boundary of the computational area (red line), inflow cell and outflow cells (blue dot and blue line), and Sybaris archaeological area (black square)

By estimating Q_p and t_p from Eqs. 11 and 12, respectively, synthetic unit hydrographs and runoff hydrographs were reconstructed for each contributing area and selected return periods. Figure 7 shows the runoff hydrographs for contributing areas A (Fig. 7a), B (Fig. 7b), and C (Fig. 7c). Peaks of discharge appeared to shift towards the left (from Fig. 7a to Fig. 7c) because of the differences in the extent of the contributing areas. This finding implied the durations of the hydrographs (47 h, 40 h, and 30 h for areas A, B, and C, respectively).

Considering contributing area A, peaks of discharge were reached after 12 h and corresponded to 907.7 m³/s, 1524.7 m³/s, 1808.4 m³/s, and 2278.9 m³/s for 10-year, 50-year, 100-year, and 300-year events, respectively. For contributing area B, peak discharges were reached after 8 h and assumed values of 453.5 m³/s, 779.6 m³/s, 930.8 m³/s, and 1182.8 m³/s for 10-year, 50-year, 100-year, and 300-year events, respectively. Finally, peak discharges were reached after 6 h for contributing area C, with values corresponding to 145 m³/s, 254.3 m³/s, 305.3 m³/s, and 390.7 m³/s for 10-year, 50-year, 100-year, and 300-year events, respectively.
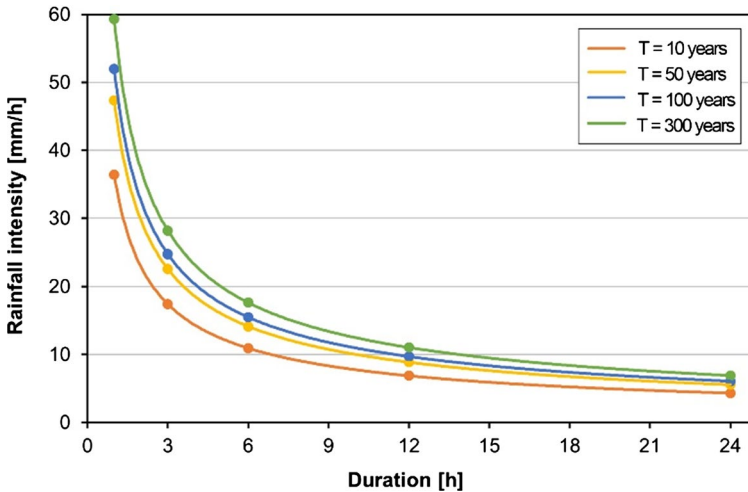
Fig. 6 IDF curves for return periods of 10, 50, 100, and 300 years

Table 4 Cumulative rainfall height (in mm) estimated for different t_c (h) and return periods (year) related to contributing areas A, B, and C

Return period	Rainfall height (mm)		
T (y)	Area A t_c 9.1 h	Area B t_c 7.2 h	Area C t_c 5.9 h
10	75.64	69.66	65.31
50	97.67	90.02	84.46
100	106.97	98.63	92.56
300	121.71	112.25	105.36

The results in terms of inundation maps depicting the extent and depth of water flow are shown in Fig. 8. As expected, the worst inundation situation occurred, often shortly, after the time of the peak of the hydrographs (≥ 2 h later) and, in particular, after 14 h, 10 h, and 7 h for contributing areas A, B, and C, respectively.

Figure 8a–d refers to contributing area A. The simulations result in the largest flooded area with no significant differences in the sizes of the inundation areas for very low to high-return periods. The Sybaris archaeological area is always affected by river overflow with water depths between a few centimetres and several metres. The Parco del Cavallo site has a flow depth of approximately 4 m for low-return periods, while Stombi, despite being located approximately 1.5 km away from the river, has a flow depth between 2 (10-year; Fig. 8a) and 4 m (300-year; Fig. 8d). Inundation maps for contributing area B (Fig. 8e–h) indicate a smaller flow extent than the previous case for low-return periods. The depth of flow reached 3 m at some parts of the Parco del Cavallo and Prolungamento Strada sites (Fig. 8e–h), while Casa Bianca and Stombi were less involved by the flow. In particular, the Stombi was not flooded for a 10-year event (Fig. 8e), while the maximum depth (almost 3 m) was observed for a 500-year event (Fig. 8h). Finally, Fig. 8i–l indicates that when considering contributing area C, the flow extent and depth in the archaeological sectors greatly reduces. For both 10-year and 50-year events (Fig. 8i, j), no significant overflows
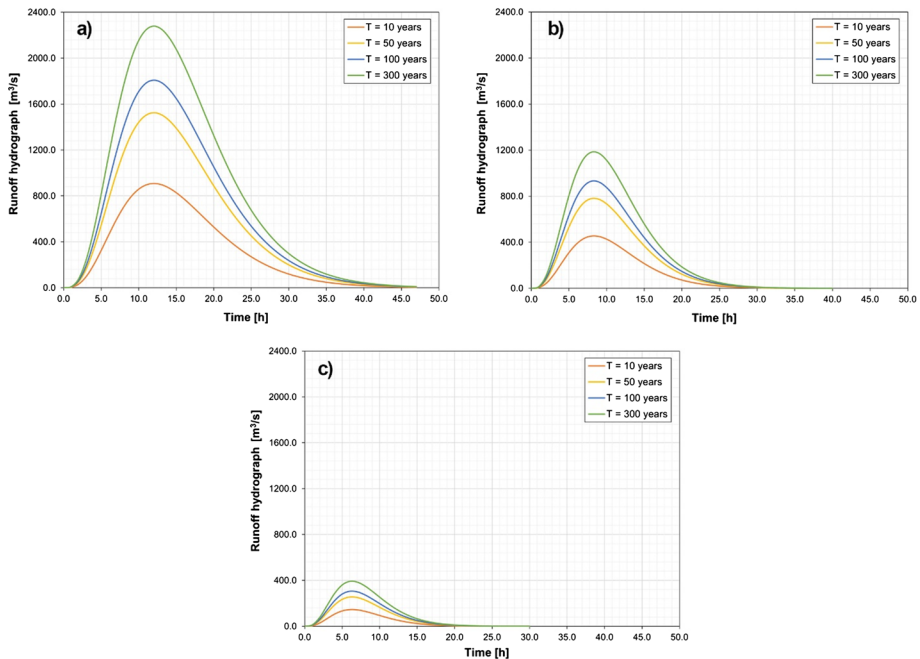
Fig. 7 Runoff hydrographs estimated for different return periods (10, 50, 100 and 300 years) and for contributing areas A (**a**), B (**b**), and C (**c**)

were observed; for a 100-year event (Fig. 8k), a limited magnitude flood (a few centimetres in depth) involved the site nearest to the river; and for a 300-year event (Fig. 8l), the flow depth reached approximately 3 m at the Parco del Cavallo and Prolungamento Strada and approximately 2 m at Casa Bianca. Otherwise, in this case, the Stombi site was never involved in flooding. The total inundation area showed a distinct decreasing trend as the return periods of the flow hydrographs decreased from contributing areas A to C.

Overlaying the inundation maps from the 300-year return period event, corresponding to the reference extreme event, to the 10-year return period event, the FH maps were assembled and classified on the basis of the corresponding return period (Fig. 9). Such a classification identify areas prone to flooding by events of specific return periods and represent a useful tool for supporting the future adoption of flood mitigation measures and the development of flood insurance plans (e.g. Linnenluecke and Griffiths 2010). In detail, the results show for contributing area A (Fig. 9a) the wider extension of the floodable area that involve the entire archaeological area, even for low-return periods. Conversely, the FH map for contributing area C (Fig. 9c) appears limited to some parts of the study area, including Parco del Cavallo, Prolungamento Strada, and Casa Bianca, for events with high-return periods (100-year and 300-year event). Even if their involvement in flooding processes depends on both the extent of the contributing area and the as-expected return period, the modelling results did not consider the long-term processes in the floodplain, such as subsidence. Subsidence is responsible for a lowering of ~ 20 mm/yr in the plain due to the neotectonic and glacio-eustatic changes and, above all, the compression of sediments (Cianflone et al. 2015). This and other external factors, such as the effects of climate change and channel adjustment, that are not considered in the FH assessment, could influence the reliability of the analysis (Whitfield
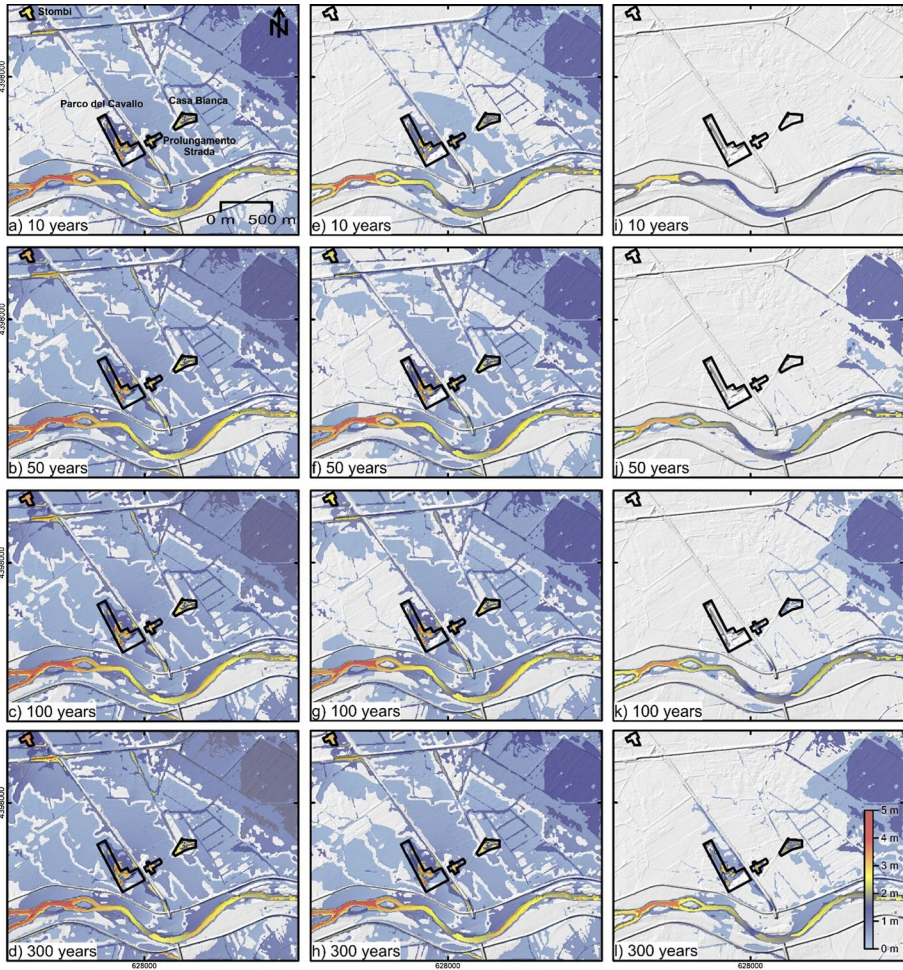
Fig. 8 Inundation maps. **a–d** for contributing area A, **e–h** for contributing area B and **i–l** for contributing area C for a 10-year, 50-year, 100-year, and 300-year events, respectively

2012; Scorpio and Rosskopf 2016; Nicholls et al. 2021) and must be considered, especially in simulations aimed at investigating long-term effects.

The main advantage related to the proposed procedure is linked to the multiscenario approach. Indeed, considering a well-defined contributing area, it was possible to reproduce the effects of localized rainfall and evaluate the potential for events with defined return periods considering only the features of the contributing area. In contrast, the common approaches consider a procedure that transformed rainfall into flood discharge (e.g. rainfall–runoff model) for which the critical rainfall is generally interpolated to cover the entire analysed basin. These methods aim to spread rainfall over the basin considering a uniformly distributed or concentrated event (e.g. areal reduction factor; Bell 1976) and only subsequently account for basin characteristics. Consequently, in the case of a large basin, these approaches could overestimate the flood discharge and

Fig. 9 FH maps for the three contributing areas considered: **a** A, **b** B, **c** C; classified on the basis of the selected return period (10, 50, 100 and 300 years)
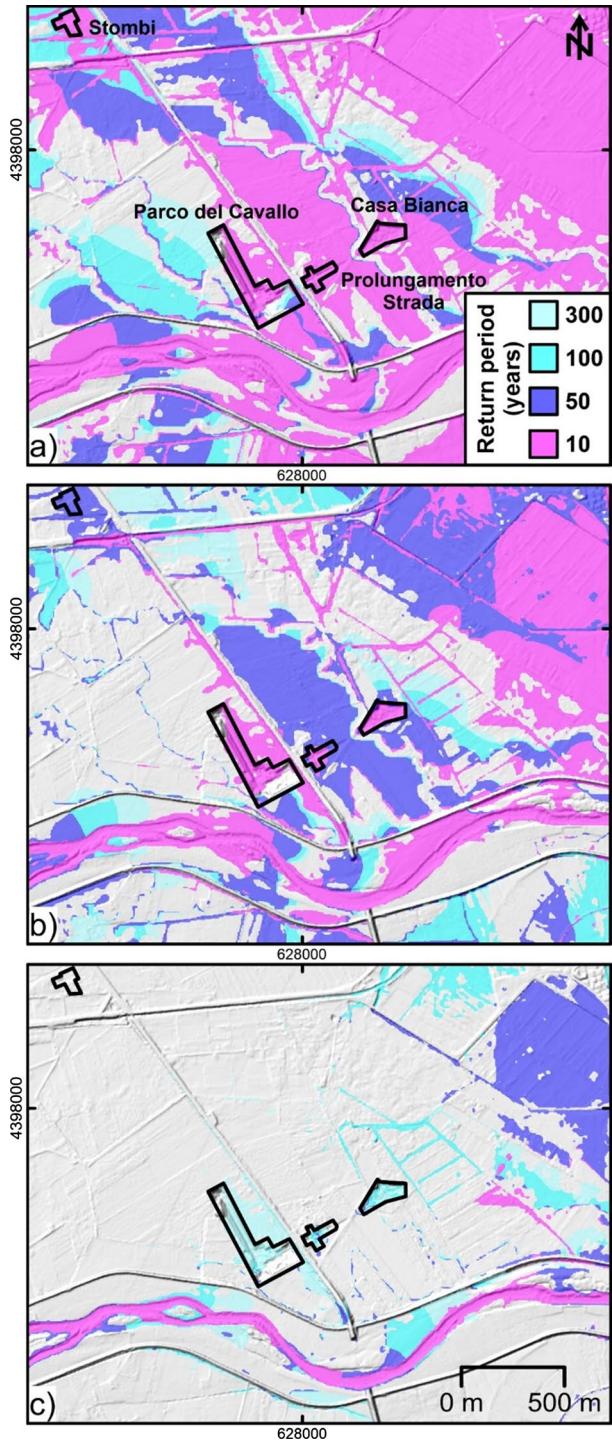
consequently hypothetical infrastructures or lead to an underestimation of them related to the hydrological and morphological characteristics of the basin.

However, there are fundamental challenges in the adoption of a multiscenario approach. One of these concerns the variability of the extent of contributing area. Indeed, in this study case, the contributing area variability was estimated by a flow-direction model based on the morphological characteristics of the basin, but it could differ if derived based on other criteria, such as a stochastic simulation or radar observations of rainfall coverage (if available).

6 Validation of estimated hydrographs

To validate the first part of the analysis results, a comparison between the runoff hydrographs estimated from the SCS-CN method and the values of the peak discharge estimated through a probabilistic analysis from the available discharge time series was conducted. This choice was related to the absence of reliable data (i.e. historical data, geomorphological field observations, or remote sensing data) indicating the area flooded in the past. Although some recent events (see 2013 and 2018 events) caused damage to the Sybaris archaeological site, only incomplete and/or large-scale reports were available (e.g. Trigila et al. 2021). Since three annual discharge time series were available, the probability of exceedance of each specific discharge was fit by the gamma distribution function (Eqs. 6, 7). By such analyses, we calculated the theoretical return period as the inverse of the probability of exceedance. Then, to describe the uncertainty in the estimation of the probability of exceedance of discharge data linked to the features of time series (i.e. sample size and continuity), 95% confidence intervals were derived on the basis of the estimated standard errors for each data series (e.g. Guerriero et al. 2020a).

Figure 10 shows gamma probability models set based on discharge data (bars) measured at the Crati (Fig. 10a), Coscile (Fig. 10b), and Esaro (Fig. 10c) hydrometric stations. Grey dots described the probability of exceedance of discharge data series; continuous lines indicated the probability model for a discharge interval defined on the basis of minimum and maximum of discharge series; overlapped triangles identified the probabilities of
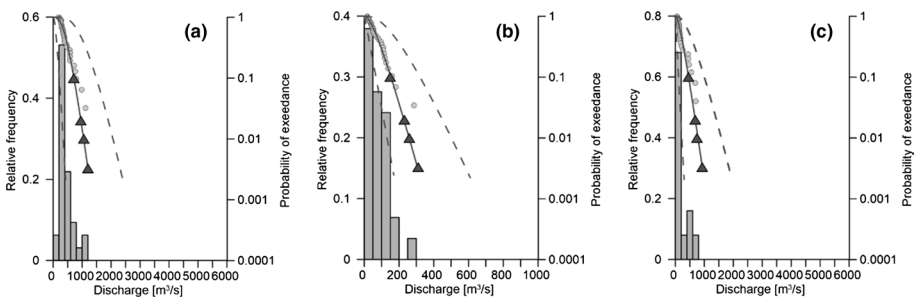

Fig. 10 Gamma probability models set on the basis of discharge data measured at the Crati (**a**), Coscile (**b**), and Esaro (**c**) hydrometric stations. Solid lines indicate the probability model; triangles indicate the probabilities of exceedance corresponding to return periods of 10 years, 50 years, 100 years, and 300 years; and dashed lines indicate 95% CIs and provide an overview of the uncertainty associated with estimated discharge

Table 5 Comparison between the discharge data derived by probability analyses of time series for the Crati, Coscile and Esaro rivers and peak discharge values for contributing areas A, B, and C derived by the runoff hydrograph for fixed return time events

Return period T (y)	Discharge (m/s)					
	Crati	Coscile	Esaro	Contributing area A	Contributing area B	Contributing area C
10	710	150	450	907	435	145
50	950	230	680	1524	779	254
100	1060	260	750	1808	930	305
300	1200	310	930	2279	1182	390

exceedance corresponding to return periods of 10 years, 50 years, 100 years, and 300 years; and 95% confidence intervals are denoted by the dashed lines.

Discharges measured for each theoretical return period are shown in Table 5. The peak values of runoff hydrographs estimated for contributing areas A, B, and C are also reported. Even if considerable uncertainty affects the estimated discharge data, especially for high-return period events, as indicated by the 95% confidence intervals (i.e. dashed lines of Fig. 10), a qualitative comparison was attempted on the basis of the return period.

The results showed that the discharge of the Crati River is comparable to the peak value modelled for the hydrographs of contributing area A, especially for low-return periods; due to the extension of contributing area B, the peak discharge could be associated with the sum of the discharges of the Coscile and Esaro Rivers, while the discharge of the Coscile River matches the peak value modelled for the hydrographs of contributing area C.

7 Conclusions

In this paper, a procedure is proposed for estimating multiscenario flood hazards in large river basins, accounting for the potential variability levels of the contributing areas related to the occurrence of meteorological concentrated events or extending over a fraction of the river basin. This approach was tested at the archaeological site of Sybaris in southern Italy by first using the SCS-CN method to derive the runoff from the rainfall on the basis of land use and soil characteristics and subsequently modelling the runoff hydrographs over the flood plain through the 2D hydrologic engineering center river analysis system (HEC-RAS) model. The runoff hydrographs were derived by intensity–duration–frequency curves (IDF) obtained by a probabilistic analysis of rainfall data. Multiple contributing areas were considered to generate runoff hydrographs for different extents of contributing areas due to the unavailability of spatial rainstorm coverage for the basin. In the presence of such data, each scenario could correspond to a predetermined extent.

The applicability and expected results of the proposed procedure are related to (1) the characteristics of the rainfall time series (i.e. number and continuity), representing the basis for a reliable fitting of the probabilistic model; (2) the features of the contributing basin regarding the extension and river characteristics and the land use and hydrological soil conditions, on which the amount of rainfall contributing to flood generation depends (derived by the rainfall–runoff model) and related data, such as land use maps and digital elevation models; and (3) uncertainties linked to the hydrodynamic model derived by the accuracy of topographic data and the impossibility of measuring

or directly estimating some parameters required by the model and the presence of validation data. However, the latter is a common issue in flood hazard analysis that can be reduced by adequate-quality hydrological input data. By considering the common availability of rainfall time history data, land cover maps, and digital elevation models, a wide applicability of the procedure is expected. A limitation of the procedure is related to the impossibility of quantitatively validating the inundation maps by historical data or geomorphological field observations. However, the same approach could be easily exported and tested in other fluvial contexts to analyse limited extension areas with available model data and historical inundation maps.

Declaration

References

Al-Abadi AM (2018) Mapping flood susceptibility in an arid region of southern Iraq using ensemble machine learning classifiers: a comparative study. Arab J Geosci 11:218. https://doi.org/10.1007/s12517-018-3584-5

Ambrosetti P, Bosi C, Carraro F et al (1987) Neotectonic map of Italy: scale 1:500000. C.N.R., Roma, Progetto Finalizzato Geodinamica

Bates PD, De Roo APJ (2000) A simple raster-based model for flood inundation simulation. J Hydrol 236:54–77. https://doi.org/10.1016/S0022-1694(00)00278-X

Bell FC (1976) The areal reduction factor in rainfall frequency estimation. Ints.Hydrol.

Bianchini S, Moretti S (2015) Analysis of recent ground subsidence in the Sibari plain (Italy) by means of satellite SAR interferometry-based methods. Int J Remote Sens 36:4550–4569. https://doi.org/10.1080/01431161.2015.1084433

Brunner GW (2021) HEC-RAS river analysis system user's manual, version 6.0. Hydrologic Engineering Center Davis, CA

Cafaro F, Cotecchia F, Lenti V, Pagliarulo R (2013) Interpretation and modelling of the subsidence at the archaeological site of Sybaris (Southern Italy). In: Bilotta E, Flora A, Lirer S, Viggiani C (eds) Geotechnical engineering for the preservation of monuments and historic sites. CRC Press, Boca Raton

do Carmo JSA (2020) Physical modelling vs. numerical modelling: complementarity and learning. https://doi.org/10.20944/preprints202007.0753.v1

Caruso C, Ceravolo R, Cianflone G et al (2013) Sedimentology and ichnology of Plio-Pleistocene marine to continental deposits in Broglio (Trebisacce, northern ionian Calabria, Italy). Mediterr Earth Sci 21:21–24

Chen Y, Li J, Xu H (2016) Improving flood forecasting capability of physically based distributed hydrological models by parameter optimization. Hydrol Earth Syst Sci 20:375–392. https://doi.org/10.5194/hess-20-375-2016

Chen Y, Barrett D, Liu R et al (2014) A spatial framework for regional-scale flooding risk assessment. In: 7th international congress on environmental modelling and software, pp 15–19

Chow VT (1959) Open-channel hydraulics. McGraw-Hill civil engineering series

Cianflone G, Tolomei C, Brunori C, Dominici R (2015) InSAR time series analysis of natural and anthropogenic coastal plain subsidence: the case of Sibari (Southern Italy). Remote Sens 7:16004–16023. https://doi.org/10.3390/rs71215812

Cianflone G, Cavuoto G, Punzo M et al (2018) Late quaternary stratigraphic setting of the Sibari Plain (southern Italy): Hydrogeological implications. Mar Pet Geol 97:422–436. https://doi.org/10.1016/j.marpetgeo.2018.07.027

Cook A, Merwade V (2009) Effect of topographic data, geometric configuration and modeling approach on flood inundation mapping. J Hydrol 377:131–142. https://doi.org/10.1016/j.jhydrol.2009.08.015

Costache R (2019) Flood susceptibility assessment by using bivariate statistics and machine learning models—a useful tool for flood risk management. Water Resour Manag 33:3239–3256. https://doi.org/10.1007/s11269-019-02301-z

De Risi R, Jalayer F, De Paola F (2015) Meso-scale hazard zoning of potentially flood prone areas. J Hydrol 527:316–325. https://doi.org/10.1016/j.jhydrol.2015.04.070

Di Baldassarre G, Schumann G, Bates PD et al (2010) Flood-plain mapping: a critical discussion of deterministic and probabilistic approaches. Hydrol Sci J 55:364–376. https://doi.org/10.1080/02626661003683389

El-Magd SAA (2019) Flash flood hazard mapping using GIS and bivariate statistical method at Wadi Bada'a, Gulf of Suez, Egypt. J Geosci Environ Protect 7:372–385. https://doi.org/10.4236/gep.2019.78025

European Environment Agency EEA (2020) CORINE land cover (CLC) 2018 version 2020_20u1. Release Date: 21-12-2018. European Environment Agency. https://land.copernicus.eu/pan-european/corine-landcover/clc2018

Ferranti L, Pagliarulo R, Antonioli F, Randisi A (2011) "Punishment for the Sinner": holocene episodic subsidence and steady tectonic motion at ancient Sybaris (Calabria, southern Italy). Q Int 232:56–70. https://doi.org/10.1016/j.quaint.2010.07.014

Furdada G, Calderón LE, Marqués MA (2008) Flood hazard map of La Trinidad (NW Nicaragua). Method and results. Nat Hazards 45:183–195. https://doi.org/10.1007/s11069-007-9156-8

Giandotti M (1934) Previsione delle Piene e delle Magre dei Corsi D'acqua; Memorie e Studi idrografici. Servizio Idrografico Italiano: Roma, Italy 8:8–13 (**In Italian**)

Gonçalves P, Marafuz I, Gomes A (2015) Flood hazard, Santa Cruz do Bispo Sector, Leça River, Portugal: a methodological contribution to improve land use planning. J Maps 11:760–771. https://doi.org/10.1080/17445647.2014.974226

Greco E, Luppino S, Munzi P (1999) Ricerche sulla topografia e sull'urbanistica di Sibari-Thuri-Copiae, pp 115–164 (**In Italian**)

Guerriero L, Focareta M, Fusco G et al (2018) Flood hazard of major river segments, Benevento Province, Southern Italy. J Maps 14:597–606. https://doi.org/10.1080/17445647.2018.1526718

Guerriero L, Ruzza G, Calcaterra D et al (2020a) Modelling prospective flood hazard in a changing climate, Benevento Province, Southern Italy. Water 12:2405. https://doi.org/10.3390/w12092405

Guerriero L, Ruzza G, Guadagno FM, Revellino P (2020b) Flood hazard mapping incorporating multiple probability models. J Hydrol 587:125020. https://doi.org/10.1016/j.jhydrol.2020.125020

Hjemfelt ATJ, Kramer LA, Burwell RE (1982) Curve numbers as random variables. Rainfall-runoff relationship. Water Resources Publications, New York

Indelicato S (1988) Verifica di modelli di valutazione del rischio idraulicogeologico ed efficacia degli interventi. Gruppo nazionale per la difesa dalle catastrofi idrogeologiche, Linea 3, Rome (**In Italian**)

Iriarte E, Sánchez MÁ, Foyo A, Tomillo C (2010) Geological risk assessment for cultural heritage conservation in karstic caves. J Cult Herit 11:250–258. https://doi.org/10.1016/j.culher.2009.04.006

Janizadeh S, Avand M, Jaafari A et al (2019) Prediction success of machine learning methods for flash flood susceptibility mapping in the Tafresh Watershed, Iran. Sustainability 11:5426. https://doi.org/10.3390/su11195426

Jenkinson AF (1955) The frequency distribution of the annual maximum (or minimum) values of meteorological elements. Q J R Meteorol Soc 81:158–171. https://doi.org/10.1002/qj.49708134804

Ji J, Choi C, Yu M, Yi J (2012) Comparison of a data-driven model and a physical model for flood forecasting. Dubrovnik, Croatia, pp 133–142

Jigyasu R, Marrion C, Poletto D, Scalet M (2014) Disaster risk management of cultural heritage sites in Albania: seismological-geohazard risk analysis and disaster risk reduction guidelines for Apollonia archaeological park, historic centres and Gjirokastra and Butrint. CNR-IGAG, Monterotondo (Roma)

Kim B-J, Kim M, Hahm D, Han KY (2021) Probabilistic flood hazard assessment method considering local intense precipitation at NPP sites. J Hydrol 597:126192. https://doi.org/10.1016/j.jhydrol.2021.126192

Liang Q, Xia X, Hou J (2016) Catchment-scale high-resolution flash flood simulation using the GPU-based technology. Procedia Eng 154:975–981. https://doi.org/10.1016/j.proeng.2016.07.585

Liberi F, Piluso E (2009) Tectonometamorphic evolution of the ophiolitic sequences from Northern Calabrian Arc. Ital J Geosci 128:483–493

Lin L, Wu Z, Liang Q (2019) Urban flood susceptibility analysis using a GIS-based multi-criteria analysis framework. Nat Hazards 97:455–475. https://doi.org/10.1007/s11069-019-03615-2

Linnenluecke M, Griffiths A (2010) Beyond adaptation: resilience for business in light of climate change and weather extremes. Bus Soc 49:477–511. https://doi.org/10.1177/0007650310368814

Magliulo P, Cusano A (2016) Geomorphology of the Lower Calore River alluvial plain (Southern Italy). J Maps 12:1119–1127. https://doi.org/10.1080/17445647.2015.1132277

Merlo C (1973) Determinazione mediante il "Metodo Razionale" delle portate massime di piena di data frequenza nei piccoli bacini. In Annali della Facoltà di Scienze Agrarie; Tipografia Vincenzo Bona: Torino, Italy **(In Italian)**

Mokhtar ES, Pradhan B, Ghazali AH, Shafri HZM (2018) Assessing flood inundation mapping through estimated discharge using GIS and HEC-RAS model. Arab J Geosci 11:682. https://doi.org/10.1007/s12517-018-4040-2

Montané A, Buffin-Bélanger T, Vinet F, Vento O (2017) Mappings extreme floods with numerical floodplain models (NFM) in France. Appl Geogr 80:15–22. https://doi.org/10.1016/j.apgeog.2017.01.002

Nicholls RJ, Lincke D, Hinkel J et al (2021) A global analysis of subsidence, relative sea-level change and coastal flood exposure. Nat Clim Change 11:338–342. https://doi.org/10.1038/s41558-021-00993-z

Nuswantoro R, Diermanse F, Molkenthin F (2016) Probabilistic flood hazard maps for Jakarta derived from a stochastic rain-storm generator. J Flood Risk Manag 9:105–124. https://doi.org/10.1111/jfr3.12114

Ongdas N, Akiyanova F, Karakulov Y et al (2020) Application of HEC-RAS (2D) for flood hazard maps generation for Yesil (Ishim) River in Kazakhstan. Water 12:2672. https://doi.org/10.3390/w12102672

Petrucci O, Polemio M (2007) Flood risk mitigation and anthropogenic modifications of a coastal plain in southern Italy: combined effects over the past 150 years. Nat Hazards Earth Syst Sci 7:361–373. https://doi.org/10.5194/nhess-7-361-2007

Ponce V, Hawkins R (1996) Runoff curve number: has it reached maturity? J Hydrol Eng. https://doi.org/10.1061/(ASCE)1084-0699(1996)1:1(11)

Puglisi S, Zanframundo P (1978) Osservazioni idrologiche in piccoli bacini del subappenino Dauno. Giornale Del Genio Civile 10–12:439–453 **(In Italian)**

Raghunath HM (2006) Hydrology: principles, analysis and design. New age international

Rahman M, Ningsheng C, Islam MM et al (2019) Flood susceptibility assessment in Bangladesh using machine learning and multi-criteria decision analysis. Earth Syst Environ 3:585–601. https://doi.org/10.1007/s41748-019-00123-y

Ramírez JA (2000) Prediction and modelling of flood hydrology and hydraulics. In: Inland flood hazards: human, riparian and aquatic communities, p 53

Rashid AA, Liang Q, Dawson RJ, Smith LS (2016) Calibrating a high-performance hydrodynamic model for broad-scale flood simulation: application to Thames Estuary, London, UK. Procedia Eng 154:967–974. https://doi.org/10.1016/j.proeng.2016.07.584

Rispoli C, Di Martire D, Calcaterra D et al (2020) Sinkholes threatening places of worship in the historic center of Naples. J Cult Herit 46:313–319. https://doi.org/10.1016/j.culher.2020.09.009

Salami AW, Bilewu SO, Ibitoye BA, Ayanshola MA (2017) Runoff hydrographs using Snyder and SCS synthetic unit hydrograph methods: a case study of selected rivers in South West Nigeria. J Ecol Eng 18:25. https://doi.org/10.12911/22998993/66258

Scorpio V, Rosskopf CM (2016) Channel adjustments in a Mediterranean river over the last 150 years in the context of anthropic and natural controls. Geomorphology 275:90–104. https://doi.org/10.1016/j.geomorph.2016.09.017

Selli R (1962) Il Paleogene nel quadro della geologia dell'Italia centro-meridionale. Mem Soc Geol Ital 3:737–789 **(In Italian)**

Shafizadeh-Moghadam H, Valavi R, Shahabi H et al (2018) Novel forecasting approaches using combination of machine learning and statistical models for flood susceptibility mapping. J Environ Manag 217:1–11. https://doi.org/10.1016/j.jenvman.2018.03.089

Soil Conservation Service (SCS) (1956, 1964, 1972, 1993) Hydrology, Section 4. In: National engineering handbook. Washington, DC, USA, USDA

Sutcliffe JV (1987) The use of historical records in flood frequency analysis. J Hydrol 96:159–171. https://doi.org/10.1016/0022-1694(87)90150-8

Teng J, Jakeman AJ, Vaze J et al (2017) Flood inundation modelling: a review of methods, recent advances and uncertainty analysis. Environ Model Softw 90:201–216. https://doi.org/10.1016/j.envsoft.2017.01.006

Tien Bui D, Hoang N-D, Pham T-D et al (2019) A new intelligence approach based on GIS-based Multivariate Adaptive Regression Splines and metaheuristic optimization for predicting flash flood susceptible areas at high-frequency tropical typhoon area. J Hydrol 575:314–326. https://doi.org/10.1016/j.jhydrol.2019.05.046

Toda LL, Yokingco JCE, Paringit EC, Lasco RD (2017) A LiDAR-based flood modelling approach for mapping rice cultivation areas in Apalit, Pampanga. Appl Geogr 80:34–47. https://doi.org/10.1016/j.apgeog.2016.12.020

Trigila A, Iadanza C, Lastoria B et al (2021) Dissesto idrogeologico in Italia: pericolosità e indicatori di rischio, 356 (**In Italian**)

Tufano R, Fusco F, De Vita P (2016) Spatial modeling of ash-fall pyroclastic deposits for the assessment of rainfall thresholds triggering debris flows in the Sarno and Lattari mountains (Campania, southern Italy). ROL 41:210–213. https://doi.org/10.3301/ROL.2016.131

Tufano R, Cesarano M, Fusco F, De Vita P (2019) Probabilistic approaches for assessing rainfall thresholds triggering landslides. The study case of the peri-Vesuvian area (southern Italy). Ital J Eng Geol Environ. https://doi.org/10.4408/IJEGE.2019-01.S-17

Tufano R, Formetta G, Calcaterra D, De Vita P (2021) Hydrological control of soil thickness spatial variability on the initiation of rainfall-induced shallow landslides using a three-dimensional model. Landslides. https://doi.org/10.1007/s10346-021-01681-x

Valagussa A, Frattini P, Crosta GB et al (2020) Hazard ranking of the UNESCO world heritage sites (WHSs) in Europe by multicriteria analysis. J Cult Herit Manag Sustain Dev 10:359–374. https://doi.org/10.1108/JCHMSD-03-2019-0023

Ventura G (1905) Bonificazione della bassa pianura bolognese: Studio sui coefficienti udometrici. Giornale Del Genio Civile 43(3):3–36 (**In Italian**)

Wang Y, Yang X (2020) A coupled hydrologic-hydraulic model (XAJ-HiPIMS) for flood simulation. Water 12:1288. https://doi.org/10.3390/w12051288

Wang Z, Lai C, Chen X et al (2015) Flood hazard risk assessment model based on random forest. J Hydrol 527:1130–1141. https://doi.org/10.1016/j.jhydrol.2015.06.008

Whitfield PH (2012) Floods in future climates: a review. J Flood Risk Manag 5(4):336–365. https://doi.org/10.1111/j.1753-318X.2012.01150.x

Woo M, Waylen PR (1986) Probability studies of floods. Appl Geogr 6:185–195. https://doi.org/10.1016/0143-6228(86)90001-9

Youssef AM, Pradhan B, Sefry SA (2015) Flash flood susceptibility assessment in Jeddah city (Kingdom of Saudi Arabia) using bivariate and multivariate statistical models. Environ Earth Sci 75:12. https://doi.org/10.1007/s12665-015-4830-8

Yue S (2001) A bivariate gamma distribution for use in multivariate flood frequency analysis. Hydrol Process 15:1033–1045. https://doi.org/10.1002/hyp.259

Web references

https://www.cfd.calabria.it/
https://www.europarl.europa.eu/32

Publisher's Note Springer Nature remains neutral with regard to jurisdictional claims in published maps and institutional affiliations.

Authors and Affiliations

Rita Tufano[1] · Luigi Guerriero[1] ⓘ **· Mariagiulia Annibali Corona[1] · Giuseppe Cianflone[2] · Diego Di Martire[1] · Fabio Ietto[2] · Alessandro Novellino[3] · Concetta Rispoli[1] · Claudia Zito[1] · Domenico Calcaterra[1]**

[1]   Department of Earth, Environmental and Resource Sciences, Federico II University of Naples, Monte Sant'Angelo Campus, Via Cintia 26, 8012 Naples, Italy

[2]   Department of Biology, Ecology and Earth Sciences, University of Study Calabria, Via P. Bucci, 15B, 87036 Arcavacata Di Rende, Cosenza, Italy

[3]   Environmental Science Centre, British Geological Survey, Keyworth, Nottingham NG12 5GG, UK